

# Equilibrium shape of single-layer hexagonal boron nitride islands on low-index metal substrates

Marin Petrović,<sup>1,2, a)</sup> Michael Horn-von Hoegen,<sup>1</sup> and Frank-J. Meyer zu Heringdorf<sup>1</sup>

<sup>1)</sup> Faculty of Physics and CENIDE, University of Duisburg-Essen, Lotharstr. 1, D-47057 Duisburg, Germany

<sup>2)</sup> Center of Excellence for Advanced Materials and Sensing Devices, Institute of Physics, Bijenička cesta 46, HR-10000 Zagreb, Croatia

Large, high-quality layers of hexagonal boron nitride (hBN) are a prerequisite for further advancement in scientific investigation and technological utilization of this exceptional 2D material. Here we address this demand by investigating chemical vapor deposition synthesis of hBN on an Ir(111) substrate, and focus on the substrate morphology, more specifically mono-atomic steps that are always present on all catalytic surfaces of practical use. From low-energy electron microscopy and atomic force microscopy data, we are able to set up an extended Wulff construction scheme and provide a clear elaboration of different interactions governing the equilibrium shapes of the growing hBN islands that deviate from the idealistic triangular form. Most importantly, intrinsic hBN edge energy and interaction with the iridium step edges are examined separately, revealing in such way the importance of substrate step morphology for the island structure and the overall quality of 2D materials.

Production of single- and multi-layer hexagonal boron nitride (hBN) samples with minimum amount of defects has developed into one of the most important areas of investigation of this insulating 2D material (2DM) exhibiting high chemical stability and excellent thermal conductivity<sup>1–3</sup>. Elimination of defects from the production process is essential for scalable, high-throughput synthesis of hBN that holds a great potential for advancements in various fields of technology, such as field effect transistors<sup>4</sup>, light-emitting diodes<sup>5</sup> and sensors<sup>6</sup>. The method enabling such synthesis is chemical vapor deposition (CVD), which in the case of hBN typically consists of initial nucleation of individual islands on a catalyst metal surface, followed by island growth and coalescence to form a full monolayer<sup>7</sup>. When neighboring islands merge, defects are formed at the boundary, resulting in lower material quality and deterioration of device performance<sup>8,9</sup>. Since island coalescence is an unavoidable step in CVD synthesis, it is important to understand all aspects of island nucleation, shape, and growth, in order to develop new routes for synthesis optimization.

Single-layer hBN has been grown via CVD on a wide range of single- and poly-crystalline metal substrates, e.g., on Ru, Rh, Ni, Ir, Pd, Pt, Cu and Fe<sup>7,10–18</sup>. Initially, hBN islands are often zig-zag (ZZ) terminated triangles, with possible exceptions for some growth conditions<sup>19–21</sup>. The triangles exhibit two dominant orientations, which originate from the bi-elemental hBN unit cell<sup>12</sup>. Further evolution of island shape, and therefore the domain boundaries later on, can be altered during CVD by adjusting the accessible parameters (e.g., temperature or precursor pressure/flux<sup>19</sup>), but the choice of a particular substrate with its specific morphology is a crucial initial factor, since precursor-substrate and hBN-substrate interactions dictate the course of the synthesis.

A very important feature of substrate morphology are surface steps. They are always present on both single-crystalline and poly-crystalline foil substrates, and are often sites of hBN nucleation<sup>22–24</sup>. Also, island growth anisotropy induced by the substrate steps has been observed for hBN on Ru(0001)<sup>25</sup>, Pt(111)<sup>26</sup>, Ir(111)<sup>23</sup>, and Cu(110)<sup>27</sup>, and in a similar manner for graphene on metals<sup>22,28,29</sup>. Due to the increased binding of the edge of 2DMs to the substrate step edge, step-up (and in some cases also step-down) growth is hindered and causes anisotropic growth rates of the islands. However, up to now very little attention has been devoted to disentangling the different energy factors that contribute to the observed island shapes. Here, we elucidate the origin of hBN island shape anisotropy on metals by performing a case study of hBN growth on Ir(111) with low-energy electron microscopy (LEEM). We explicitly consider the intrinsic energy of hBN island edges<sup>30</sup>, the islands' binding to the substrate, and the specifics of the interaction between hBN island and substrate step edges. Such detailed study is feasible because hBN-Ir interaction is weak enough to allow hBN growth over the step edges, but is sufficiently strong<sup>31</sup> so that the effects of hBN edge-Ir step edge interaction become clearly visible in experiments in the form of distinct triangular and trapezoidal islands with ZZ edges<sup>23</sup>.

Single-layer hBN was grown on Ir(111) in an ultra-high vacuum setup via CVD by using borazine as a precursor. The Ir single-crystal was cleaned by Ar sputtering at 2 keV followed by heating in oxygen at 1170 K and annealing at 1470 K. Unless otherwise noted, the borazine pressure during CVD was  $10^{-8}$  mbar and the temperature was 1170 K. An Elmitec SPE-LEEM III microscope was used to carry out *in-situ*, bright field LEEM and selected-area low-energy electron ( $\mu$ -LEED) measurements. Atomic force microscope (AFM) measurements were performed *ex-situ* in air with a Veeco Dimension 3100 microscope operated in tapping mode.

LEEM images in Figs. 1(a) and (b) show isolated hBN

<sup>a)</sup> Electronic mail: mpetrovic@ifs.hr

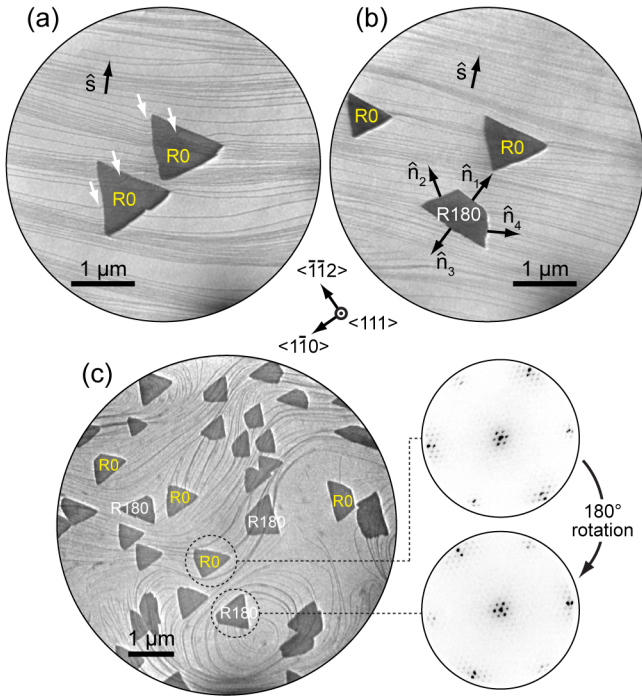


Figure 1. (a) and (b) LEEM images of hBN islands on Ir(111) with uniform  $\hat{s}$  (designating Ir step-up direction). White arrows indicate sites of strong Ir step edge bending. Edge normals  $\hat{n}_i$  are noted for one of the islands in panel (b). (c) LEEM image of R0 and R180 islands, including two representative  $\mu$ -LEED patterns, on a part of the Ir surface with strongly varying  $\hat{s}$ . (a) and (b)  $E = 24.1$  eV, (c)  $E = 17.5$  eV in LEEM and  $E = 35.2$  eV in  $\mu$ -LEED. Crystallographic directions noted in the center of the figure apply to all LEEM and LEED images.

islands on the Ir surface, where thin dark lines spanning across the field of view are Ir step edges. Crystallographic analysis, taking into account image rotation in LEEM (e.g., see Ref. 21 for technical details), reveals that the hBN edges are of ZZ type. The orientation of hBN island edges can be described by unit vectors  $\hat{n}$  which are perpendicular to the edges, as shown in Fig. 1(b). The local orientation of Ir steps is designated by a unit vector  $\hat{s}$  which for every point along the step is perpendicular to the step. The orientation of  $\hat{s}$ , i.e., the difference between step-up and step-down direction, can be determined by recognizing that the short base of the trapezoid must be facing the Ir step-up direction (see AFM data below). When straight steps are present on the Ir surface and  $\hat{s}$  shows minor change across a large area, as in Fig. 1(a) and (b), one hBN orientation (denoted as R0) grows exclusively in triangular form, and the other one (rotated by  $180^\circ$ , denoted as R180) grows exclusively in the form of trapezoids, as we reported earlier<sup>23</sup>. The shape of islands changes, however, when the Ir substrate exhibits a complex surface morphology and contains step edges with large curvature, including hills and valleys. Such a situation is shown in Fig. 1(c), where many R0 and R180

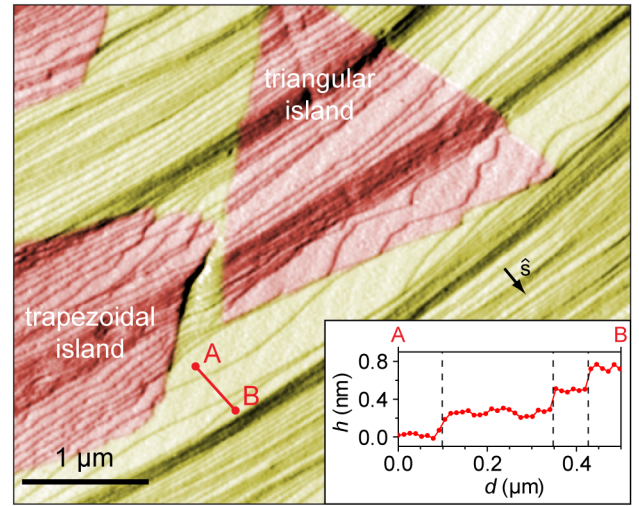


Figure 2. AFM image (first derivative of topography in  $x$ ) of hBN islands (red) on Ir(111) (yellow). Thin diagonal lines are Ir step edges. The inset shows line profile between points A and B prior to AFM image differentiation, vertical dashed lines mark positions of Ir step edges.

islands are visible (in this particular case, the borazine pressure during synthesis was  $6 \times 10^{-8}$  mbar, leading to a higher island density). Whether the islands are of R0 or R180 orientation can be deduced (i) by simply measuring the orientation of their edges, or (ii) by comparing the islands' 3-fold symmetric  $\mu$ -LEED patterns as illustrated in Fig. 1(c).

A careful inspection of LEEM images reveals that R0 islands are triangular on some parts of the surface, while they are trapezoidal on other parts [see labeled islands in Fig. 1(c)]. Moreover, the short base of trapezoidal islands is found at different positions, i.e., the triangles truncation occurs at different vertices, in order to form trapezoids. This is also valid for R180 islands. Considering that the short base of trapezoidal islands faces the step-up direction of Ir, we deduce that R0 and R180 islands are not predetermined to grow as triangles or trapezoids, but their shape is governed by Ir step morphology.

Close to the hBN edges, Ir steps are often strongly bent, as marked by white arrows in Fig. 1(a), indicating that the interaction between hBN island edges and Ir step edges is significant and plays an important role in the growth of hBN. Recently, Poelsema et al. also found that the growth of hBN on Ir(111) results in a severe reorientation of Ir step edges<sup>32</sup>. A better view of step layout can be obtained from scanning probe imaging. In Fig. 2, an AFM image with several hBN islands is shown. The step-up direction is easily identified from an AFM profile shown in the inset. Ir step edges, which are rather straight in the hBN-free region, are distorted in areas where hBN islands overgrew them. This is most prominent at the lower right edge of the triangular island that faces the Ir step-up direction, where Ir steps exhibit a wavy structure and contain straight segments parallel to

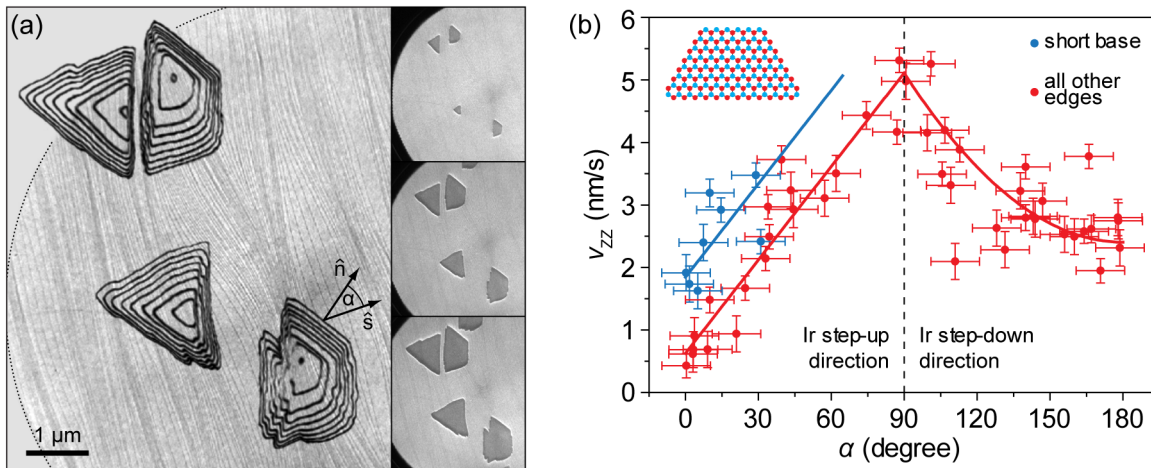


Figure 3. (a) Stacked contours of hBN islands extracted from a LEEM growth sequence, three characteristic images are shown in the panels on the right. Contours correspond to islands perimeters recorded at time intervals of 32 s. Edge normal  $\hat{n}$ , local step-up direction  $\hat{s}$  and an angle between them  $\alpha$  are noted for one hBN edge.  $E = 17.3$  eV. (b) Data plot of ZZ edge advancement speed  $v_{ZZ}$  as a function of angle  $\alpha$ . Red and blue lines are the fits to the data.

the hBN edge. Furthermore, in Fig. 2, a short base of the trapezoidal island has formed in the step-up direction, facilitating in such way parallel configuration of hBN edge and Ir steps. Our AFM data suggests that strong hBN-Ir interaction favors attachment of hBN edges to Ir step edges which is enabled by their parallel alignment, most prominently in the step-up direction of Ir.

We now proceed to discuss the evolution of the island shape during growth. Contours of several hBN islands extracted from LEEM data are shown in Fig. 3(a), corresponding to the ZZ-type perimeters of R0 and R180 islands recorded at time intervals of 32 s. The island growth is quantified by measuring edge distances from the island nucleation site,  $d$ , and calculating the average advancement speed as  $v_{ZZ} = d/t$ . At the same time, the angle  $\alpha$  between  $\hat{n}$  and  $\hat{s}$  has been measured for each edge, thus providing information to plot  $v_{ZZ}$  as a function of  $\alpha$ . In total, 16 islands have been analyzed, and from the data shown in Fig. 3(b) it is clear that hBN edges propagate faster (slower) when their normals  $\hat{n}$  are perpendicular (parallel) to the local direction of  $\hat{s}$ . Short bases of trapezoids (blue dots) have been singled out from all other edges (red dots) because of their different elemental composition (see inset). The data in Fig. 3(b) shows functional dependence, and we fit it with simple mathematical functions in order to establish an analytical model of hBN growth. At  $\alpha = 90^\circ$ , the island edge changes its growth orientation from step-up to step-down with respect to the Ir surface, and it is reasonable to assume modification of hBN-Ir interaction and also a different behavior of  $v_{ZZ}(\alpha)$ . Therefore, we fit the data with a combination of linear (for  $\alpha \leq 90^\circ$ ) and quadratic (for  $\alpha > 90^\circ$ ) functions (see Supporting Section S1 for fit details).

From a comparison of the product  $v_{ZZ}L$ , where  $L$  is the typical island size, with the values of the diffusion coeffi-

cient  $D$  of various borazine fragments, i.e., the building blocks for hBN growth, it is clear that  $D \gg v_{ZZ}L$  (see Supporting Section S2 for more details). This implies that hBN growth on Ir(111) is taking place near the thermodynamic equilibrium and that  $v_{ZZ}$  is proportional to the edge free energy<sup>33</sup>. In that case, the thermodynamic Wulff construction can be applied to obtain the shape of 2D islands<sup>33,34</sup>, and hence we use it to reconstruct the observed R0 and R180 island forms. We use an analytic expression for the epitaxial hBN island edge energy per unit length as a function of polar angle and chemical potential difference,  $\gamma(\chi, \Delta\mu)$ <sup>30,34</sup> (see Supporting Section S3 for details). The chemical potential  $\Delta\mu$  is defined as a disbalance between chemical potentials of B and N atoms,  $\Delta\mu = (\mu_B - \mu_N)/2$ . Highly positive  $\Delta\mu$  favors B-terminated ZZ edges, while highly negative  $\Delta\mu$  favors N-terminated ZZ edges.  $\gamma(\chi, \Delta\mu)$  also contains binding energies of ZZ and armchair edges to Ir that can be found in the literature<sup>24,35,36</sup>.

To be consistent with the realistic experimental values of  $\Delta\mu$ <sup>36</sup>, and also with the preference of B-terminated ZZ edges<sup>23,24</sup>, our analysis is restricted to  $1.5 \text{ eV} < \Delta\mu < 3 \text{ eV}$ . A comparable analysis with N-terminated island edges, where  $\Delta\mu < 0$ , is straightforward. The Wulff construction of an hBN island at  $\Delta\mu = 1.8 \text{ eV}$  is shown in the polar plot in Fig. 4(a). The edge energy  $\gamma(\chi, \Delta\mu)$  used in this construction includes the hBN island's intrinsic edge energy and the binding of hBN to the flat Ir substrate without steps (details are given in the Supporting Section S3). The island shape is determined by the red points of  $\gamma(\chi, \Delta\mu)$  which correspond to B-terminated ZZ edges. N-terminated ZZ edges, designated by blue points, have higher energy and therefore do not constitute the edges of hBN island at these conditions. It follows from Fig. 3 and the outlined diffusion considerations that  $v_{ZZ}(\alpha)$  corresponds to the ZZ edge energy modulation arising



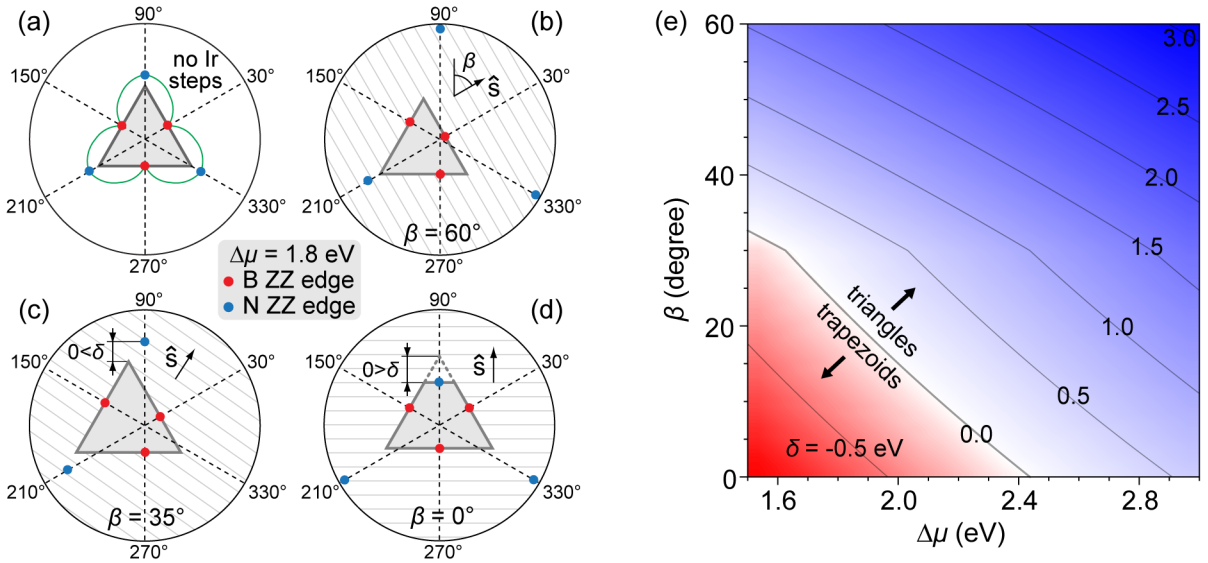


Figure 4. (a) Thermodynamic Wulff construction of an hBN island on Ir without steps. Green line is  $\gamma(\chi, \Delta\mu)$ , and gray triangle indicates the Wulff shape. (b)-(d) Transition of a triangular island shape to trapezoidal after including the interaction of hBN with the Ir steps and subsequent rotation of  $\hat{s}$ . Gray lines indicate Ir steps. (e) Plot of  $\delta(\beta, \Delta\mu)$ . For  $\delta < 0$  (red region) and  $\delta > 0$  (blue region), trapezoidal and triangular islands grow on the Ir surface, respectively.

from the relative edge orientation with respect to the Ir steps. This is incorporated into the Wulff construction by applying  $\gamma(\chi, \Delta\mu) \rightarrow \gamma(\chi, \Delta\mu) \cdot v_{ZZ}(\chi)$  and by repositioning the red and the blue points in Figs. 4(b)-(d) accordingly. Our LEEM data shows that these few points are the only relevant ones to describe the shape of hBN islands.

For the sake of clarity, we focus on the top vertex and the upper-right edge of the triangular hBN island in Figs. 4(a)-(d) to examine the truncation effect of the island. Introduction of Ir steps modifies the energies of all hBN edges, depending on the orientation of hBN island with respect to Ir steps. This orientation is quantified by the angle  $\beta$  measured between  $\hat{s}$  and direction corresponding to  $\chi = 90^\circ$  [see Fig. 4(b)]. For relatively large values of  $\beta$  as in Figs. 4(b) and (c), Ir step-bending as visible in the AFM data of Fig. 2 is the optimal mechanism for hBN island energy minimization. The required bending at the upper-right island edge is not large (step energy increases with the step curvature<sup>37</sup>) and its cost is compensated by an overall energy gain achieved by strong binding between parallel hBN edge and Ir steps. In such a situation, B-terminated ZZ edges remain energetically preferred. As  $\beta$  decreases, the cost of Ir step bending becomes too high and it becomes energetically non-profitable. However, the energy of N-terminated ZZ edge at the top of the island in Fig. 4(d) is reduced significantly since it becomes (nearly) parallel with Ir steps, resulting in hBN island truncation at the vertex pointing in the step-up direction. After truncation, at the short base of the trapezoidal island, it takes much less (if any) Ir step bending to achieve a parallel configuration and strong binding between hBN island edge and Ir steps,

and in such way an initially unfavorable N-termination of hBN islands is energetically compensated.

The presented Wulff construction predicts, in agreement with our LEEM data, that the truncation is allowed only in the Ir step-up direction. It can be argued that in the step-up direction hBN edges become passivated by binding to metal atoms. The result of such an interaction would be a much stronger binding in the step-up direction as compared to the step-down direction, similarly to the case of epitaxial graphene<sup>29</sup>. Binding of different hBN edges to Ir steps that undergo bending and repositioning constitutes the energetic background of  $v_{ZZ}(\alpha)$ , and that is why the inclusion of  $v_{ZZ}(\alpha)$  into the Wulff construction is crucial for obtaining the experimentally observed shapes of hBN islands.

A systematic investigation of the truncation effect is shown in Fig. 4(e) in which  $\delta$ , i.e., the vertical separation between N-terminated ZZ edge and its closest vertex as depicted in Figs. 4(c) and (d), is plotted as a function of  $\Delta\mu$  and  $\beta$ . For certain  $(\beta, \Delta\mu)$  combinations, trapezoidal islands ( $\delta < 0$ , red region) are energetically preferred over triangular ones ( $\delta > 0$ , blue region). This explains why R0 and R180 islands have different shapes on the surface with uniform  $\hat{s}$ , and also why do they change their shape when  $\hat{s}$  (i.e.,  $\beta$ ) changes. The level of truncation of the triangle also depends on  $\Delta\mu$  and  $\beta$ , explaining trapezoids of different heights in Fig. 1(c).

In summary, we have shown that the step morphology of the substrate used in CVD growth of hBN is a crucial factor which determines the energetically most stable shape of synthesized hBN islands. The total energy of the system is minimized by adhering hBN edges to the Ir step edges, which is achieved by repositioning of

Ir steps and formation of trapezoids (instead of triangles) during hBN growth. The degree of Ir step repositioning and the feasibility of trapezoidal shape depend on the relative orientation between hBN island edges and Ir steps, and the chemical potentials of B and N atoms during the synthesis of hBN. The use of an extended Wulff construction allowed exact pinpointing of different energy contributions governing hBN growth, and this enables the application of our results, by adjusting the relevant interaction parameters, in studies of hBN synthesis on other metal substrates.

See Supporting information for details of the  $v_{ZZ}(\alpha)$  data fit, evaluation of the diffusion coefficients, and details of  $\gamma(\chi, \Delta\mu)$ .

The Alexander von Humboldt Foundation is acknowledged for financial support. M.P. would like to thank Thomas Michely for stimulating discussions.

## REFERENCES

- <sup>1</sup>A. Nagashima, N. Tejima, Y. Gamou, T. Kawai, and C. Oshima, *Phys. Rev. Lett.* **75**, 3918 (1995).
- <sup>2</sup>A. Pakdel, Y. Bando, and D. Golberg, *Chem. Soc. Rev.* **43**, 934 (2014).
- <sup>3</sup>K. Zhang, Y. Feng, F. Wang, Z. Yang, and J. Wang, *J. Mater. Chem. C* **5**, 11992 (2017).
- <sup>4</sup>T. Roy, M. Tosun, J. S. Kang, A. B. Sachid, S. B. Desai, M. Hettick, C. C. Hu, and A. Javey, *ACS Nano* **8**, 6259 (2014).
- <sup>5</sup>J. S. Ross, P. Klement, A. M. Jones, N. J. Ghimire, J. Yan, D. G. Mandrus, T. Taniguchi, K. Watanabe, K. Kitamura, W. Yao, D. H. Cobden, and X. Xu, *Nat. Nanotechnol.* **9**, 268 (2014).
- <sup>6</sup>M. Sajjad, G. Morell, and P. Feng, *ACS Appl. Mater. Interfaces* **5**, 5051 (2013).
- <sup>7</sup>K. K. Kim, A. Hsu, X. Jia, S. M. Kim, Y. Shi, M. Hofmann, D. Nezich, J. F. Rodriguez-Nieva, M. Dresselhaus, T. Palacios, and J. Kong, *Nano Lett.* **12**, 161 (2012).
- <sup>8</sup>A. L. Gibb, N. Alem, J.-H. Chen, K. J. Erickson, J. Ciston, A. Gautam, M. Linck, and A. Zettl, *J. Am. Chem. Soc.* **135**, 6758 (2013).
- <sup>9</sup>Q. Li, X. Zou, M. Liu, J. Sun, Y. Gao, Y. Qi, X. Zhou, B. I. Yakobson, Y. Zhang, and Z. Liu, *Nano Lett.* **15**, 5804 (2015).
- <sup>10</sup>A. Goriachko, He, M. Knapp, H. Over, M. Corso, T. Brugger, S. Berner, J. Osterwalder, and T. Greber, *Langmuir* **23**, 2928 (2007).
- <sup>11</sup>M. Corso, W. Auwärter, M. Muntwiler, A. Tamai, T. Greber, and J. Osterwalder, *Science* **303**, 217 (2004).
- <sup>12</sup>W. Auwärter, M. Muntwiler, J. Osterwalder, and T. Greber, *Surf. Sci.* **545**, L735 (2003).
- <sup>13</sup>Y.-H. Lee, K.-K. Liu, A.-Y. Lu, C.-Y. Wu, C.-T. Lin, W. Zhang, C.-Y. Su, C.-L. Hsu, T.-W. Lin, K.-H. Wei, Y. Shi, and L.-J. Li, *RSC Adv.* **2**, 111 (2012).
- <sup>14</sup>F. Orlando, R. Larciprete, P. Lacovig, I. Boscarato, A. Baraldi, and S. Lizzit, *J. Phys. Chem. C* **116**, 157 (2012).
- <sup>15</sup>M. Morscher, M. Corso, T. Greber, and J. Osterwalder, *Surf. Sci.* **600**, 3280 (2006).
- <sup>16</sup>E. Čavar, R. Westerström, A. Mikkelsen, E. Lundgren, A. Vinogradov, M. L. Ng, A. Preobrajenski, A. Zakharov, and N. Mårtensson, *Surf. Sci.* **602**, 1722 (2008).
- <sup>17</sup>S. Joshi, D. Ecija, R. Koitz, M. Iannuzzi, A. P. Seitsonen, J. Hutter, H. Sachdev, S. Vijayaraghavan, F. Bischoff, K. Seufert, J. V. Barth, and W. Auwärter, *Nano Lett.* **12**, 5821 (2012).
- <sup>18</sup>N. A. Vinogradov, A. A. Zakharov, M. L. Ng, A. Mikkelsen, E. Lundgren, N. Mårtensson, and A. B. Preobrajenski, *Langmuir* **28**, 1775 (2012).
- <sup>19</sup>Y. Stehle, H. M. Meyer, R. R. Unocic, M. Kidder, G. Polizos, P. G. Datskos, R. Jackson, S. N. Smirnov, and I. V. Vlassiouk, *Chem. Mater.* **27**, 8041 (2015).
- <sup>20</sup>B. Poelsema, A. Acun, L. Schouten, F. Derkink, M. Tsvetanova, Z. Zhang, H. J. W. Zandvliet, and A. van Houselt, *2D Materials* **6**, 035010 (2019).
- <sup>21</sup>J. Felter, M. Raths, M. Franke, and C. Kumpf, *2D Materials* **6**, 045005 (2019).
- <sup>22</sup>P. W. Sutter, J.-I. Flege, and E. A. Sutter, *Nat. Mater.* **7**, 406 (2008).
- <sup>23</sup>M. Petrović, U. Hagemann, M. Horn-von Hoegen, and F.-J. Meyer zu Heringdorf, *Appl. Surf. Sci.* **420**, 504 (2017).
- <sup>24</sup>F. H. Farwick zum Hagen, D. M. Zimmermann, C. C. Silva, C. Schlueter, N. Atodiresci, W. Jolie, A. J. Martínez-Galera, D. Dombrowski, U. A. Schröder, M. Will, P. Lazić, V. Caciuc, S. Blügel, T.-L. Lee, T. Michely, and C. Busse, *ACS Nano* **10**, 11012 (2016).
- <sup>25</sup>P. Sutter, J. Lahiri, P. Albrecht, and E. Sutter, *ACS Nano* **5**, 7303 (2011).
- <sup>26</sup>Y. Zhang, X. Weng, H. Li, H. Li, M. Wei, J. Xiao, Z. Liu, M. Chen, Q. Fu, and X. Bao, *Nano Lett.* **15**, 3616 (2015).
- <sup>27</sup>L. Wang, X. Xu, L. Zhang, R. Qiao, M. Wu, Z. Wang, S. Zhang, J. Liang, Z. Zhang, Z. Zhang, W. Chen, X. Xie, J. Zong, Y. Shan, Y. Guo, M. Willinger, H. Wu, Q. Li, W. Wang, P. Gao, S. Wu, Y. Zhang, Y. Jiang, D. Yu, E. Wang, X. Bai, Z.-J. Wang, F. Ding, and K. Liu, *Nature* **570**, 91 (2019).
- <sup>28</sup>E. Loginova, N. C. Bartelt, P. J. Feibelman, and K. F. McCarty, *New J. Phys.* **11**, 063046 (2009).
- <sup>29</sup>Z.-J. Wang, J. Dong, Y. Cui, G. Eres, O. Timpe, Q. Fu, F. Ding, R. Schloegl, and M.-G. Willinger, *Nat. Commun.* **7**, 13256 (2016).
- <sup>30</sup>Y. Liu, S. Bhowmick, and B. I. Yakobson, *Nano Lett.* **11**, 3113 (2011).
- <sup>31</sup>A. Preobrajenski, M. Nesterov, M. L. Ng, A. Vinogradov, and N. Mårtensson, *Chem. Phys. Lett.* **446**, 119 (2007).
- <sup>32</sup>B. Poelsema, H. J. W. Zandvliet, and A. van Houselt, *New Journal of Physics* (2019), 10.1088/1367-2630/ab3dda.
- <sup>33</sup>V. I. Artyukhov, Y. Liu, and B. I. Yakobson, *Proc. Natl. Acad. Sci. U.S.A.* **109**, 15136 (2012).
- <sup>34</sup>Z. Zhang, Y. Liu, Y. Yang, and B. I. Yakobson, *Nano Lett.* **16**, 1398 (2016).
- <sup>35</sup>R. Laskowski, P. Blaha, and K. Schwarz, *Phys. Rev. B* **78**, 045409 (2008).
- <sup>36</sup>R. Zhao, F. Li, Z. Liu, Z. Liu, and F. Ding, *Phys. Chem. Chem. Phys.* **17**, 29327 (2015).
- <sup>37</sup>M. Giesen, *Prog. Surf. Sci.* **68**, 1 (2001).